

Article

Emerging PAT for Freeze-Drying Processes for Advanced Process Control

Alex Juckers ^{1,2} , Petra Knerr ², Frank Harms ² and Jochen Strube ^{1,*}

¹ Institute for Separation and Process Technology, Clausthal University of Technology, 38678 Clausthal-Zellerfeld, Germany

² Martin Christ Gefriertrocknungsanlagen GmbH, 37520 Osterode am Harz, Germany

* Correspondence: strube@itv.tu-clausthal.de

Abstract: Lyophilization is a widely used drying operation, but long processing times are a major drawback. Most lyophilization processes are conducted by a recipe that is not changed or optimized after implementation. With the regulatory demanded quality by design (QbD) approach, the process can be controlled inside an optimal range, ensuring safe process conditions. Process analytical technology (PAT) is crucial because it allows real-time monitoring and is part of a control strategy. In this work, emerging PAT (manometric temperature measurement (MTM), comparative pressure measurement, heat flux sensors, and ice ruler) are used for measurements during the freeze-drying process, and their potential for implementation inside a control strategy is outlined.

Keywords: lyophilization; process analytical technology (PAT); quality by design (QbD); process control

1. Introduction

Lyophilization process design and optimization generally rely on trial and error, causing a high experimental workload and processes with optimization potential [1–3]. In order to ensure efficiency and assist innovation in the development and manufacturing of pharmaceuticals, a systemic approach demanded by regulatory authorities has been introduced [4,5]. Quality by design (QbD) has three basic components: quality assurance by developing robust formulations and processes, scientific understanding of the impact of formulation and process on the product, and capability for continuous improvement. It is a systematic development approach that starts with predefined goals and focuses on product and process understanding as well as process control based on science and risk management [1]. Product quality is achieved by designing an effective and efficient manufacturing process. The benefits of QbD are reduced manufacturing costs, faster time to market, and reduced regulatory burden because changes do not need prior approval. An exemplary QbD workflow is shown in Figure 1.

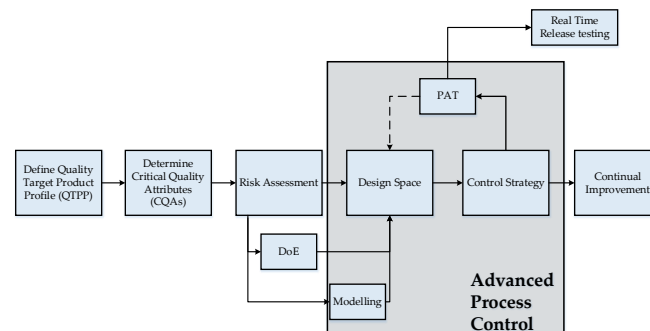


Figure 1. QbD process development workflow [6].



Citation: Juckers, A.; Knerr, P.; Harms, F.; Strube, J. Emerging PAT for Freeze-Drying Processes for Advanced Process Control. *Processes* **2022**, *10*, 2059. <https://doi.org/10.3390/pr10102059>

Academic Editor: Jie Zhang

Received: 16 September 2022

Accepted: 9 October 2022

Published: 12 October 2022

Publisher's Note: MDPI stays neutral with regard to jurisdictional claims in published maps and institutional affiliations.



Copyright: © 2022 by the authors. Licensee MDPI, Basel, Switzerland. This article is an open access article distributed under the terms and conditions of the Creative Commons Attribution (CC BY) license (<https://creativecommons.org/licenses/by/4.0/>).

First, the critical quality attributes (CQA) have to be examined. Drug potency and storage stability are of utmost importance. Since lyophilization consists mainly of three steps: freezing, primary, and secondary drying, the critical process parameters (CPPs) for every step have to be identified. In the freezing step, the liquid water is transformed into ice, and the solute is either crystallized or vitrified. Here the shelf temperature, cooling rate, and the mechanism of nucleation (uncontrolled vs. controlled) are CPPs because they influence the freezing rate and ice growth. Primary and secondary drying share the same CPPs: shelf temperature, chamber pressure, and step duration. During primary drying, the solid ice is sublimed to vapor. For sublimation to occur, the chamber pressure has to be decreased under the equilibrium vapor pressure of the ice. Since sublimation is an endothermic process, heat has to be supplied to the product by the shelf. The combination of the controlled shelf temperature and chamber pressure determines the temperature profile inside the product. The product temperature must not exceed the critical value of the formulation in order to sustain an elegant product. The duration of the primary drying is critical since, in the secondary drying, the shelf temperature is increased. Leftover ice would cause collapse and rejection of the batch. During the secondary drying, bound water inside the solute matrix is separated by desorption. Shelf temperature, chamber pressure, and duration are critical for the final setting of the residual moisture. It is important to note that the CPPs can be varied throughout the different steps and do not have to be kept at a constant value. The CQAs and CPPs are summarized in Table 1.

Table 1. Critical quality attributes and process parameters in lyophilization [1,7].

Critical Quality Attributes	Critical Process Parameters
Product integrity and stability	Freezing
	Shelf temperature
	Cooling rate
Drug potency	Uncontrolled vs. controlled nucleation
	Primary drying
	Shelf temperature
Reconstitution time	Chamber pressure
	Duration
Cake appearance	Secondary Drying
	Shelf temperature
	Chamber pressure
	Duration

Next, a risk assessment identifies the most important formulation and processing factors that impact product quality [7,8]. Here, different tools can be used. Ishikawa diagrams show impact factors based on categories, while occurrence impact diagrams provide a quantitative rating of severity and frequency. Failure mode effect analysis is also a powerful tool for the detection of impact factors. Here severity, occurrence, and detection are combined into a risk preference number.

In the design space, operating parameters are defined that ensure product quality. To establish the design space, multiparameter optimization is necessary. A systematic experimental approach aimed at establishing appropriate limits for important formulation and process variables is required. In the definition of the design, space modeling is also a powerful tool since it can reduce the experimental workload significantly based on a few preliminary experiments [7,9].

Process analytical technology (PAT) is a crucial part of QbD as it is based on the use of real-time process monitoring and control as part of an overall control strategy. The FDA defines PAT as a “system for designing, analyzing and controlling manufacturing through timely measurements of critical quality and performance attributes of raw and in-process materials and processes with the goal of ensuring final product quality” [4]. The adequate use of PAT tools can provide crucial information for process understanding, continuous improvement, and relevant knowledge relating to physical, chemical, and

biological properties. Potential effects of PAT on the process are reduced cycle times, increased automation, improvement of energy and material use, capacity increase, and real-time release.

2. Process Analytical Technology for Lyophilization

Especially for lyophilization, a wide variety of PAT is available. During primary drying, the determination of product temperature, sublimation rate, and the primary drying endpoint are favorable. The PAT can be classified into different categories: single vial vs. batch or invasive vs. noninvasive.

2.1. Single Vial PAT

Thermocouples (TCs) or Resistance Thermal Detectors (RTDs) are most commonly used to measure the product temperature of selected vials during the drying process. With Thermocouples, the product temperature is measured by the Seebeck effect. Two unequal metal wires touch at the tip, and the measured voltage can be correlated to a product's temperature. For precise measurement of the product temperature, the tip of the sensor has to be at the bottom. TCs are not compatible with automatic loading systems of freeze-dryers and have to be inserted by an operator leading to a sterility risk. The electrical resistance of the metals inside the RTD is temperature dependent and can be measured with a Wheatstone bridge. The measurement is robust and precise, but the wires are challenging for loading as well, and the temperature sensing region is relatively big distributed over the whole sensor leading to average temperature data. RTDs are more frequently used in manufacturing [10].

Newer technologies measure the product temperature wireless, e.g., TEMPRIS or WTMplus. They are powered by the excitation of a passive transponder, and the resonance of the quartz crystal inside the sensor is temperature-dependent [11]. Further advantages are compatibility with automatic loading systems, flexibility in the placement, and sterilization. Different temperature sensors are shown in Figure 2.

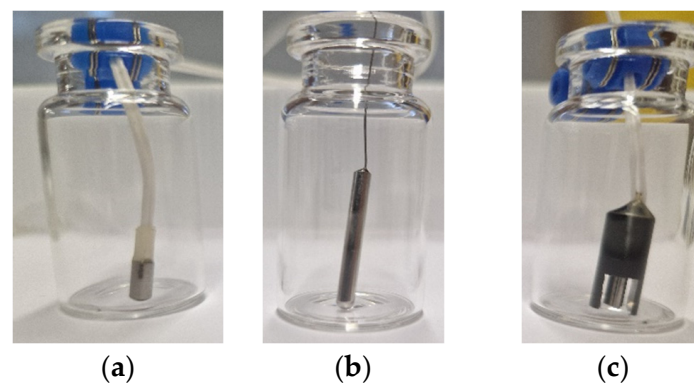


Figure 2. Different temperature sensors in 6R Vials: (a) PT100, (b) WTMplus, and (c) RTD.

Heat flux transducers are able to measure the heat flow between the shelf and the vial. They are, therefore, able to give insights into different thermal events during lyophilization, such as nucleation, ice crystal growth, sublimation, desorption, and general temperature ramps [12]. The sensor consists of an array of thermocouples mounted close to the bottom and the top surface of the transducer and is attached between the shelf and vial bottom with a high conductive tape [13]. The temperature gradient between thermocouples indicates the amount and direction of heat flow. Placement and high conductivity are important for the measurement.

Spectroscopic methods such as near-infrared and Raman can also be used to monitor single vials during lyophilization. At characteristic frequencies, IR radiation can excite molecules, and the reflectance of a sample is measured by scanning several wavelengths. Since water is a permanent dipole, it can be easily monitored using NIR. The sensor is placed

near the side bottom of the vial [14]. During the different steps of the lyophilization process, significant spectral changes can be detected [15,16]. The freezing point, ice formation process, the transition from frozen to dried material, and precise primary and secondary drying endpoint can be detected [17]. NIR can indicate critical product characteristics such as the secondary structure of protein and the residual moisture. It is a nondestructive, noninvasive, and rapid technique, but it needs accurate calibration [18].

Raman is also able to indicate different critical product and process characteristics, such as product crystallization, solid-state characteristics of intermediate and end products, and endpoints of freezing and primary drying [19,20]. It is also noninvasive and analyzes the process in real time. In contrast to NIR, the Raman probe is placed above the product to be lyophilized.

Since water and ice produce weak Raman but strong NIR spectra, both PATs can be used simultaneously on two different vials to prevent saturation of the Raman signal by NIR reflectance.

2.2. Batch PAT

A capacitance pressure sensor is able to measure the chamber pressure during the lyophilization process. It consists of an isolated chamber that is separated from the drying chamber by a membrane. Inside the isolated chamber, a defined vacuum of less than 10^{-7} Torr is applied to serve as zero reference pressure [18]. The pressure difference between the drying chamber and the isolated chamber leads to a deflection of the membrane resulting in a measurable voltage that is directly proportional to the chamber pressure. The capacitance sensor measures the absolute pressure and is independent of gas composition. It has excellent measurement accuracy and can be steam sterilized.

Pirani sensors can also be used for the measurement of the chamber pressure, but their pressure reading is highly dependent on gas composition. Here, a constantly heated wire is cooled by the gas atmosphere. At low pressures, the heat transfer rate from the wire is directly proportional to the pressure, and the pressure can be determined by the wire resistance. Pirani sensors are less expensive than capacitive sensors but less accurate.

The schematic design of both sensors is depicted in Figure 3.

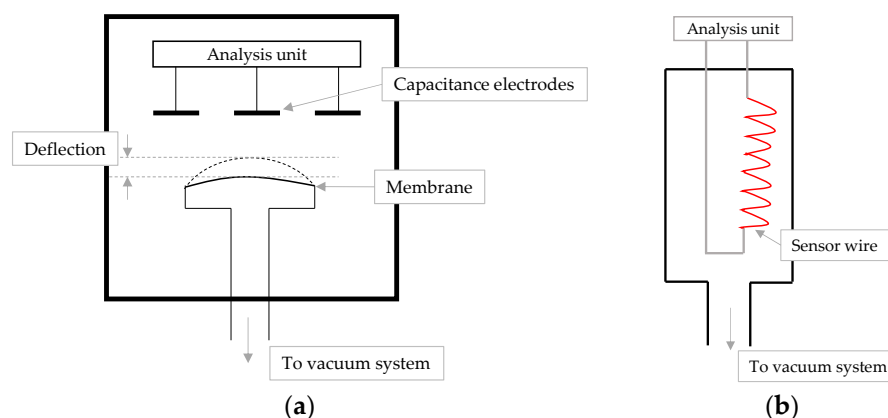


Figure 3. Schematic design of (a) capacitance sensor and (b) Pirani sensor.

The combination of Pirani and capacitance pressure sensors allows the application of a comparative pressure measurement [18]. During primary drying, the gas inside the drying chamber mainly consists of water. It has a higher heat capacity than nitrogen; therefore, the Pirani sensor shows a higher pressure than the capacitance sensor. As soon as primary drying is finished, the gas composition shifts from mainly water to nitrogen. This shift leads to a change in pressure reading, signaling the end of primary drying [21–23].

Mass spectrometry (MS) or residual gas analysis (RGA) can be applied to monitor the water concentration inside the drying chamber. A quadrupole MS is used to identify gases based on their mass-to-charge ratio. The gas is brought into the instrument, where

it is fragmented, ionized, and accelerated in an electric field. The ions are sampled by a detector that gives a proportional signal to the concentration and type of impacting fragment. For quantitative measurement, elaborate calibration is necessary [17]. It can be installed with a sterile aseptic filter to allow usage in production [24]. It has a high sensitivity but is expensive. In addition to the detection of water, it can discover the presence of pump oil, residual and cleaning solvents, heat transfer fluid, and outgassing of elastomeric components.

Manometric temperature measurement (MTM) is a PAT that is based on analyzing pressure rise data. The valve in the duct separating the drying and ice condenser chamber is closed periodically for a short time. The resulting pressure rise data are collected and analyzed using the MTM equation [25,26]:

$$p(t) = p_i - (p_i - p_0) \cdot \exp\left[-\left(\frac{3.461 \cdot N \cdot A_p \cdot T_s}{V \cdot (R_p + R_s)}\right) \cdot t\right] + 0.465 \cdot p_i \cdot \Delta T \cdot \left[1 - 0.811 \cdot \exp\left(-\frac{0.114}{L_{frozen}} \cdot t\right)\right] + X \cdot t \quad (1)$$

where $p(t)$ is chamber pressure increase during the pressure rise test, p_0 is the chamber pressure at the start of the test, p_i is the equilibrium vapor pressure of ice, N is the number of vials, V is the drying chamber volume, ΔT is the product temperature difference between the sublimation interface and the ground, and X is a variable for the linear pressure increase.

Several factors influence the pressure rise. The initial rise is caused by continuous sublimation from the vials until the equilibrium vapor pressure is established and is controlled by the product resistance. Subsequent mechanisms are fast temperature equilibration along the ice layer, causing temperature increase at the sublimation front, and the continuous heating of ice by shelves since less heat is removed by sublimation leading to a possible increase in product temperature of up to 2 °C. Another small contribution is leaking in the chamber. The contributions to the pressure rise during MTM are summarized in Figure 4.

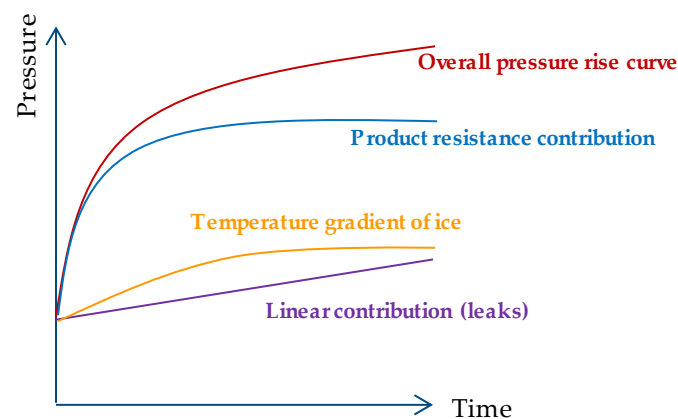


Figure 4. Contributions to pressure rise during MTM.

MTM yields the vapor pressure of ice at the sublimation interface and the dry layer resistance. During MTM, the chamber pressure increases to the equilibrium vapor pressure value of the coldest vials since it is the lowest; further sublimation would recondense water vapor on colder vials [25]. Batch heterogeneity can significantly deviate the results since the number of vials sublimating is unclear. Usually, the R_p value is only valid until approx. two-thirds of primary drying is finished since, here, the first vials are finished with sublimation [27], but the p_i value remains useful.

Tunable diode laser absorption spectroscopy (TDLAS) noninvasively measures the real-time mass flow rate of water. The beams' wavelength is set to the water absorption line and transmitted through the gas, and the absorption is measured [28].

The unit is installed in the duct that connects the drying and ice condenser chambers. Usually, two laser beams are installed: one with and the other directed against the vapor flow (s. Figure 5).

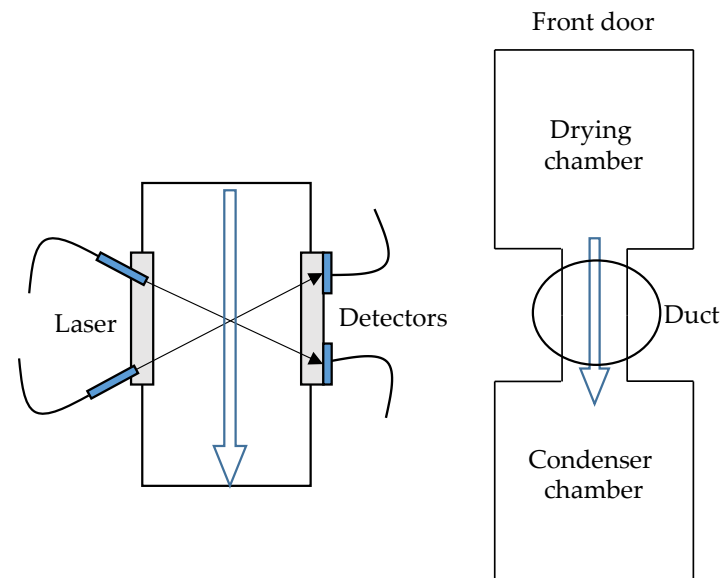


Figure 5. TDLAS setup inside a freeze dryer.

This allows the determination of water vapor concentration, and through the Doppler shift of the spectra, the gas velocity can be specified [20]. Together with the knowledge of the cross-sectional area of the duct, the calculation of the water vapor mass flow rate is possible. Furthermore, TDLAS allows the determination of the vial heat transfer coefficient [29]. TDLAS can only be installed in freeze dryers that have sufficient length, and the evolving gas flow profile in the duct must be considered for optimal measurement.

Table 2 shows some literature studies for different PAT tools.

Table 2. Studies of different PAT.

PAT	Literature
NIR and Raman	[14,15,30–41]
Heat flux	[12,13,42–45]
Comparative pressure	[7,9,21,28,46–48]
MS	[16,18,47,49]
MTM	[2,7,9,18,26,28,47,50–54]
TDLAS	[55–61]

In this work, different PAT tools are shown, and their potential for process control is outlined: Comparative pressure measurement, MTM, Heat flux, and the newly developed ice ruler are used with different concentrations of an amorph and crystalline solute, and the results are discussed.

3. Materials and Methods

3.1. Product Mixture and Instruments

Mannitol solutions were prepared with d-mannitol ($\geq 98\%$, Sigma-Aldrich, St. Louis, MO, USA) and saccharose solutions with d(+)-saccharose (vwr) in purified water (ariumTMpro, Sartorius AG, Göttingen, Germany) based on the required concentration by the experiment. A laboratory-scale LC 1200 S (Sartorius AG, Göttingen, Germany) is used to measure the weights. Product solutions of 5, 25, and 100 g/L have been used.

3.2. Freeze Drying Experiments

An Epsilon 2-6D LSCplus pilot scale freeze dryer (Martin Christ Gefriertrocknungsanlagen GmbH, Osterode am Harz, Germany) is used for freeze-drying experiments. 6R vials are used as containers for freeze-drying. An Eppendorf Research plus 0.5–5 mL pipette (Eppendorf AG, Hamburg, Germany) is used to fill 2 mL in a total of 270 vials before loading onto the middle and top shelf. The product temperature during all phases of freeze-drying is measured by Wireless Temperature Measurement plus (WTMplus) sensors. The freeze-drying recipe is depicted in Table 3. In the last primary drying step, comparative pressure measurement is used as a forwarding condition. Secondary dry does not start until the forwarding condition of 15% is fulfilled.

Table 3. Freeze-drying recipe for product solutions.

	Shelf Temperature [°C]	Pressure [mbar]	Duration [hh:mm]
Freezing	20 → −45	1000	01:05
	−45	1000	01:00
	−45		00:01
Primary drying	−45 → −30		00:15
	−30	0.15	08:00
Secondary drying	−30 → 40		02:20
	40		12:00

3.3. Heat Flux Sensor

Heat flux measurements have been made using an FHF03 economical foil heat flux sensor with thermal spreaders (Hukseflux Thermal Sensors, Delft, The Netherlands). A thermopile measures the temperature difference across the sensor area. It has a sensing area of 2.5 cm² and a sensor thickness of 0.8 mm. The sensor is placed on the front left side to measure the vial 1.1 (s. Figure 6) and fixed with Scotch[®] adhesive tape 8915 (3M Deutschland GmbH, Neuss, Germany). Measured data are collected with LI-19 software (Hukseflux Thermal Sensors, Delft, The Netherlands).



Figure 6. Position of heat flux sensor FHF03 in the freeze dryer.

3.4. Ice Ruler

The ice ruler is a ruler that is attached to the pipe of the ice condenser. It consists of a 3D-printed holder that has a ruler attached to it. During the freeze-drying process, the ice ruler is observed by a LyoCam through the sight window of the ice condenser. The arrangement is shown in Figure 7. Different intervals for photography can be assigned

in the LPCplus software (Martin Christ Gefriertrocknungsanlagen GmbH, Osterode am Harz, Germany).

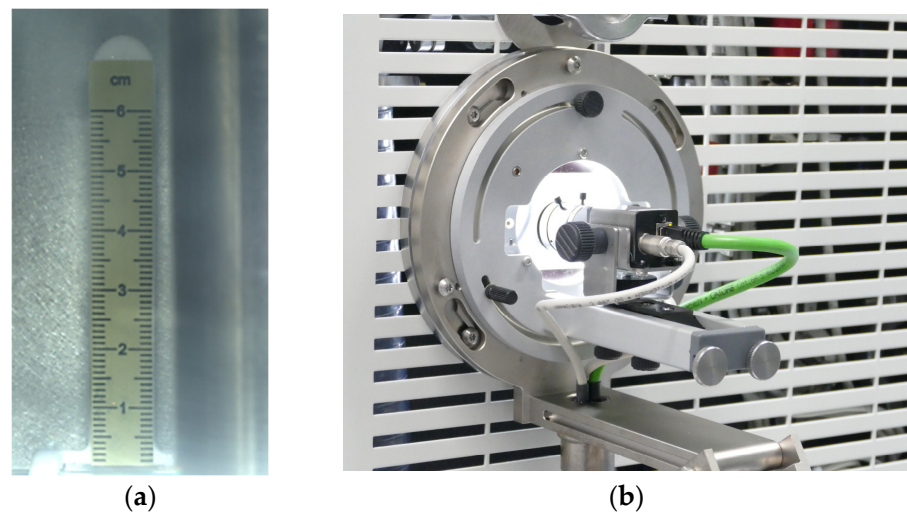


Figure 7. (a) Ice ruler and (b) position of LyoCam for observation.

3.5. Vial Heat Transfer

The vial heat transfer coefficient K_V is determined by ice sublimation tests. This procedure yields individual values for K_V . The 6R vials are filled with water and loaded onto the shelf. Selected vials are weighed before the freeze-drying procedure is started. The shelf temperature and chamber pressure of the primary drying phase have been varied. The shelf temperature setpoints are -25 , -12.5 , and 0 °C, while the chamber pressure is set to 0.05, 0.1, 0.15, and 0.3 mbar. Primary drying is aborted after around 4 h. The selected vials are weighed again after thawing.

$$K_v = \frac{(\Delta m \cdot \Delta H_s) / \Delta t}{A_v \cdot (T_S - T_p)} \quad (2)$$

Δm describes the mass difference, ΔH_s is the sublimation enthalpy, Δt is the primary drying duration, A_v is the outer cross-sectional area of the vial, and T_S and T_p are the shelf and product temperature.

During this experiment, the heat flux sensor obtained data for the heat flux, and the K_v value was additionally obtained.

3.6. Dry Layer Resistance

The dry layer resistance R_p is determined by an optimized periodic MTM. Every 10 min, the measurement takes place lasting for up to 30 s, depending on the pressure rise. During MTM, the increase in chamber pressure leads to an increased heat transfer and could possibly damage the product. The optimized measurement has the advantage that the temperature increase in the product is low because the measurement is aborted as soon as no pressure rise is detected for 3 s.

4. Results

4.1. WTMplus

The WTMplus sensors are used for product temperature measurement. They are placed in the middle on the bottom of the vial with the aid of a guide for accurate measurement. During the freezing step, the product temperature decreases, and during primary drying, the product temperature slightly increases. After all ice is sublimated, a sudden rise in product temperature can be seen. Product temperature curves are depicted in Figure 8.

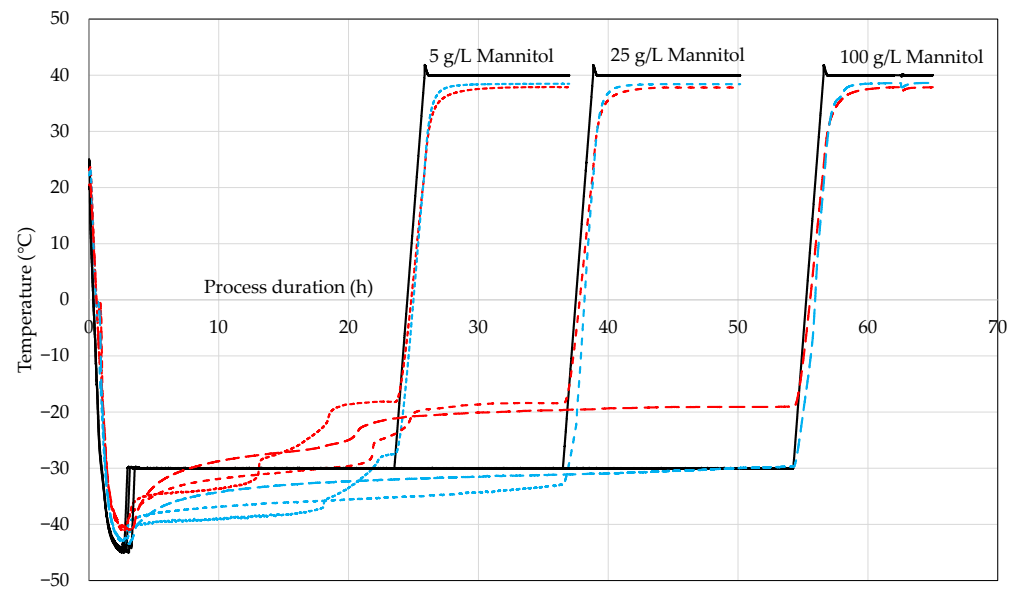


Figure 8. Temperature curves of freeze-drying run with different solute concentrations (black—shelf temperature, blue—center vial, and red—edge vials).

With the aid of WTMplus sensors, the dynamic of the freeze-drying process can be seen. Edge and center vials dry at different speeds. This is due to the so-called edge effect. Vials on the outside of the shelf receive a higher radiative heat input and therefore dry faster and at higher temperatures, leading to a significant batch heterogeneity. With increased solute concentration, center and edge vials dry at higher temperatures. Here the dry layer resistance is higher, and therefore the sublimation rate is slower, leading to an increase in product temperature. The batch heterogeneity increases further with higher solute concentrations (s. Table 4).

Table 4. Relative batch heterogeneity for different experiments.

Substance	Concentration (g/L)	Relative Batch Heterogeneity (-)
Sucrose	5	49.41%
	25	56.32%
	100	59.08%
Mannitol	5	35.00%
	25	43.59%
	100	58.26%

4.2. Comparative Pressure Measurement

Comparative pressure can be used for the endpoint determination of the whole batch. In this study, it is used as a forwarding condition. The last step of the primary drying phase is finished after the recipe, and then comparative pressure checks for the forwarding condition. If it has already fallen below the condition, secondary drying is started, but if the condition is not met, the primary drying step is continued. The value of the forwarding condition is set to 15%. This value lies at the midpoint of the capacitive rise and therefore comprises a safe process condition (s. Figure 9). The pressure sensors detect the increase in pressure during the pressure rise test, as can be seen by the fluctuations of the signal, but the comparative pressure value stays stable all the time, showing the robustness of the forwarding condition throughout the primary drying.

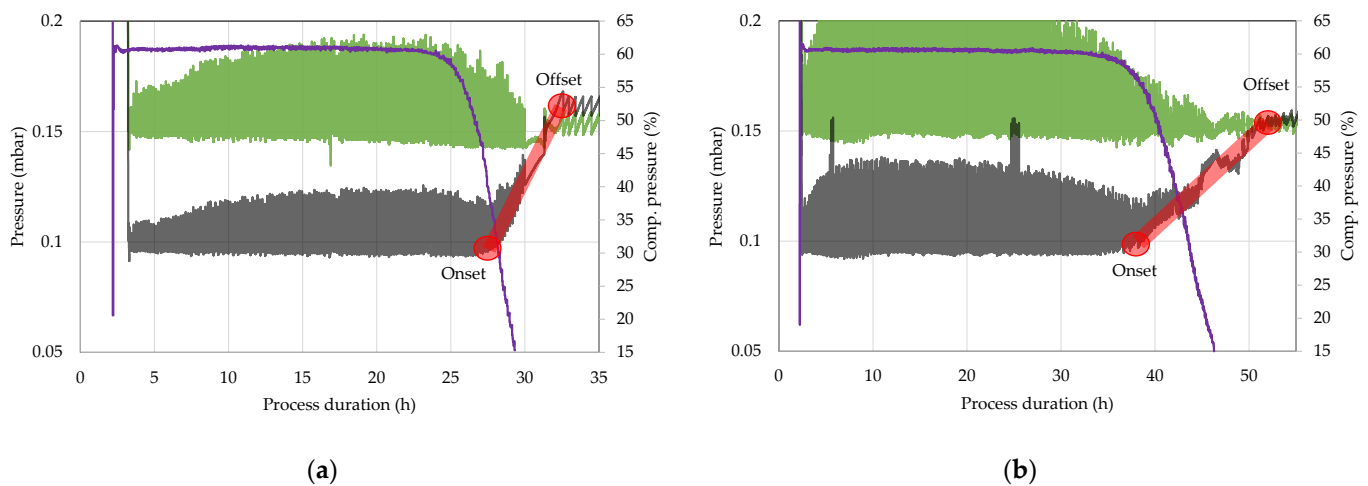


Figure 9. Comparative pressure measurement for (a) 5 g/L saccharose and (b) 100 g/L saccharose (green—Pirani sensor, black—capacitive sensor, and violet—comparative pressure).

Comparative pressure measurement can also be used for the quantitative assessment of batch heterogeneity. A high batch heterogeneity leads to a slower shift of the gas atmosphere than a low heterogeneity, causing a slower capacitive approach to the Pirani sensor. The onset and offset of the capacitive sensor are used for the evaluation. The onset is the point where the pressure value first starts increasing. The offset is the point where the increase stops, and the new stationary pressure value is established. With 5 g/L Saccharose, there is a much steeper increase in the capacitive pressure value than with 100 g/L since, here, the batch heterogeneity is smaller. Between the onset and offset are 5 h (5 g/L) and 14 h (100 g/L).

4.3. MTM

MTM is an adaptation of the pressure rise test yielding valuable data for process development and control. With the aid of MTM, the dry layer resistance of the product solution can be determined. It is a necessary model parameter for different modeling approaches. The first values of R_p are outside of the 95% confidence interval. This is mainly due to the reason that at the start of primary drying, not all vials start to sublime at the same point. As discussed before, the edge vials start earlier with the sublimation process compared with the center vials because they have a higher energy input that leads to a temperature rise inside the frozen product. The sublimation process starts as soon as the temperature-dependent vapor pressure of ice exceeds the chamber pressure. This lag in the sublimation process leads to a higher dry layer resistance because the number of vials alters from the actually sublimating vials inside the freeze dryer in the MTM equation. As soon as all vials start sublimating, the dry layer value decreases and then shows a progressive increase with rising dry layer height. It has to be kept in mind that the MTM value for R_p is only valid until two-thirds of the primary drying time because, at this point, the first vials have finished primary drying. This point is detectable by a significant increase in R_p . Here the number of vials again alters from the actual number of sublimating vials, leading to an overestimation of R_p . In Figure 10, the dry layer resistance for 25 g/L for varying process conditions is shown. The experiment with a shelf temperature of $-12.5\text{ }^{\circ}\text{C}$, chamber pressure of 0.1 mbar, and a fill volume of 1.5 mL has been conducted three times to allow statistical evaluation, while the other experiments are performed once. At first, the R_p values for the single experiments increase very sharply and show a value of about 50,000 m/s. This value then decreases. The sharp increase to the higher value is caused by batch heterogeneity. The edge vials are drying earlier than the center vials; therefore, in the beginning, the R_p value is overestimated. As soon as all vials sublime R_p decreases, the experimentally determined R_p value is in good agreement. With changing process conditions, the dry layer resistance can still be reliably determined for a given product

solution. Therefore, MTM is an optimal tool for the online determination of the dry layer resistance R_p .

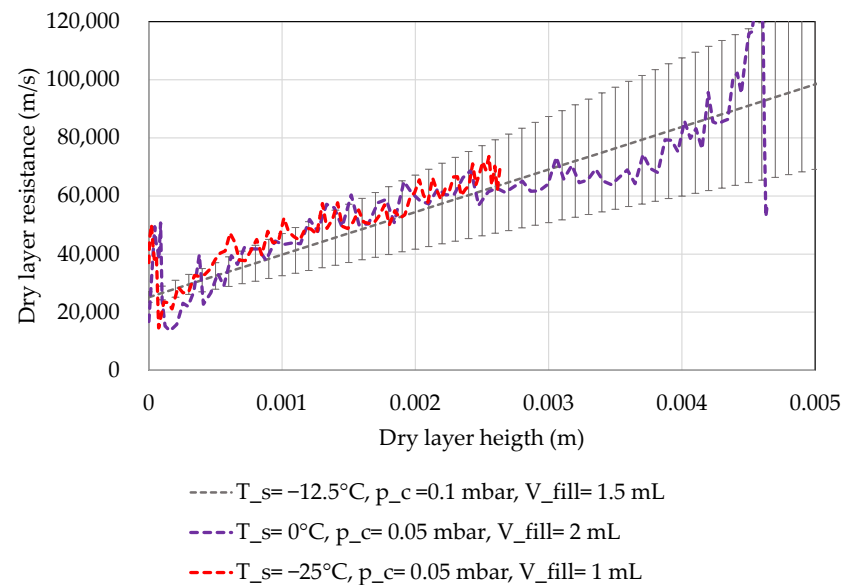


Figure 10. Experimentally determined R_p values with varying process conditions for 25 g/L saccharose.

The R_p of a formulation depends on the solute concentration. With increasing solute concentration, R_p increases for both solutes (s. Figure 11), leading to a lower sublimation rate that prolongs the primary drying process. For 5 g/L mannitol, the initial R_p value is 37,000 m/s and for 100 g/L mannitol 50,000 m/s. R_p increases linearly for 5 g/L to a final value of 130,000 m/s, while it increases sharply to 160,000 m/s for 100 g/L and then stays constant. At higher concentrations, saccharose has a lower dry layer resistance of 130,000 m/s and dries faster, whereas, at low concentrations, mannitol shows slightly lower resistance and dries here faster. It can be easily seen that formulation and process development is an integrated process to achieve an optimal process for the product while conserving the CQAs.

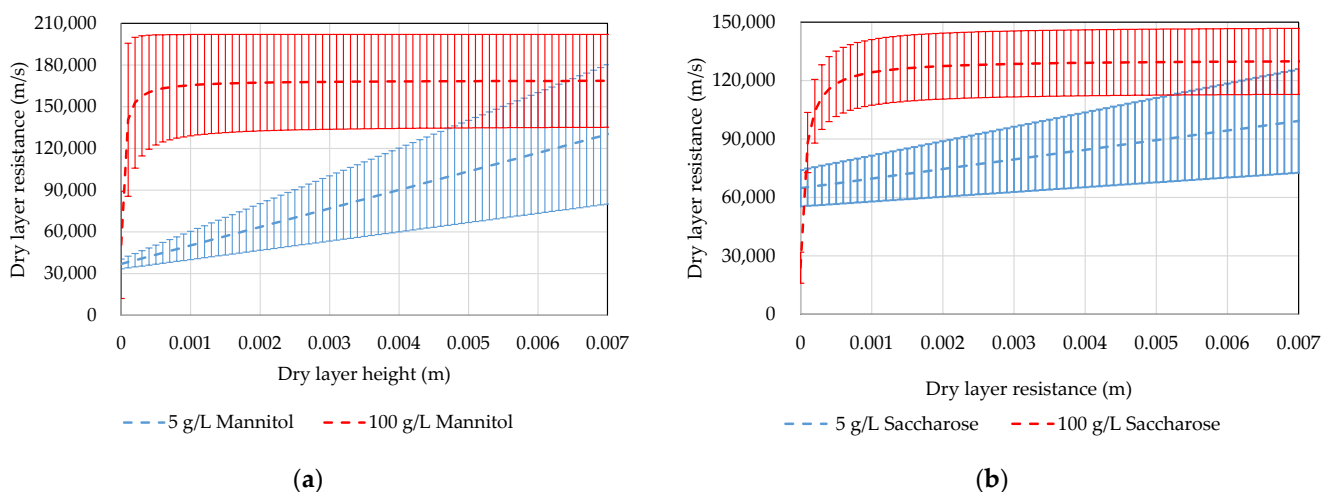


Figure 11. Dry layer resistance for different solute concentrations at the same process conditions: (a) Mannitol (b) Saccharose.

MTM can be used for endpoint determination of primary drying processes. As soon as all ice is sublimated, no pressure increase can be detected in the chamber; therefore, the equilibrium pressure of ice equals the chamber pressure. Since MTM is a batch method, the

endpoint is compared to the comparative pressure measurement onset. In Figure 12, the determined endpoints are depicted in a parity diagram. MTM and comparative pressure measurement show good agreement. Saccharose solutions dry faster at higher solute concentrations, while mannitol is faster at low concentrations. MTM shows, for all solute concentrations, a slightly faster endpoint of primary drying. It can be used as an orthogonal tool to determine the endpoint of primary drying and can be used as a complimentary forwarding condition.

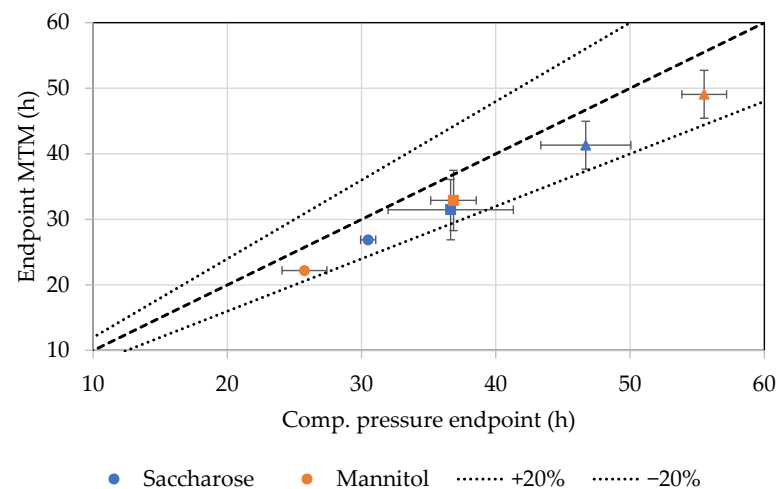


Figure 12. Primary drying endpoint of MTM and comparative pressure measurement (round—5 g/L, square—25 g/L, and triangle—100 g/L).

During the measurement, the chamber pressure inside the drying chamber increases. The increased chamber pressure leads to accelerated heat transfer into the product, increasing the product temperature. This could lead to collapse if the product temperature is near the critical temperature. The duration of the measurement is usually 25–30 s. Here, an optimized manometric temperature measurement is used. As soon as no significant pressure increase is detected, the pressure rise test is aborted. This leads to minimal temperature increase while obtaining all necessary information. In Figure 13, the necessary measurement time is shown. The measurement time is around 5.7 s and only increases at the end of primary drying but is always lower than the static standard time of 25–30 s.

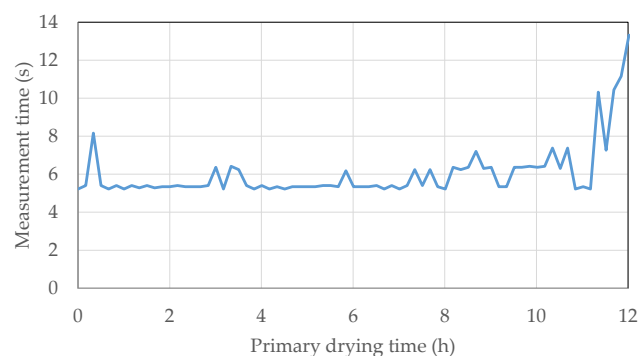


Figure 13. Measurement time for MTM during primary drying for 25 g/L Saccharose, T_s —0 °C, and p_c —0.15 mbar.

4.4. Heat Flux

The heat flux sensor is able to detect different thermal events during the lyophilization process. During the freezing step, the product is cooled with a specific cooling rate. Heat is transferred from the warmer vial into the colder shelf. Here, the temperature difference is approximately 3 °C. After a certain period and some degree of supercooling, nucleation

of ice crystals begins (here at approx. 7 h). This is detected by the heat flux sensor with a significant increase in the transferred heat flow, resulting in a product temperature rise to around $-1\text{ }^{\circ}\text{C}$. Ice crystal growth is another exothermic event that can be detected. The frozen solution is then further cooled to the final freezing temperature. Figure 14 shows the resulting heat flux signals with the corresponding product temperature.

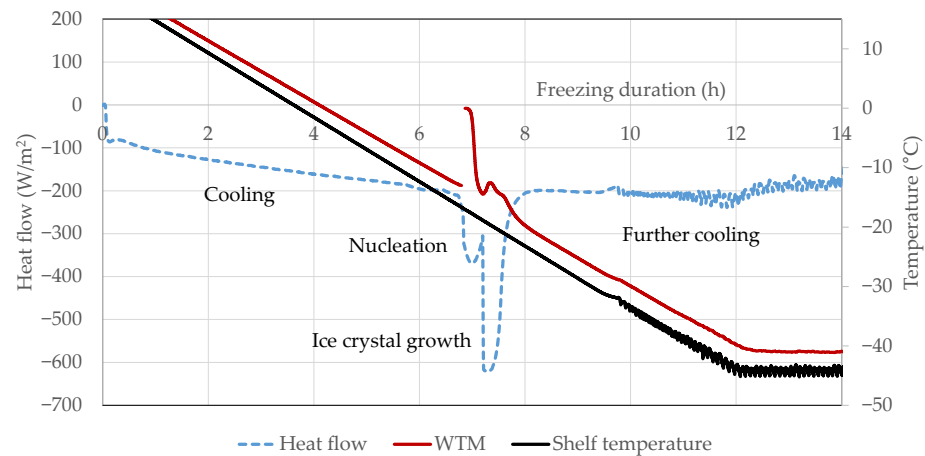


Figure 14. Heat flux and product temperature data for the freezing step of water.

During primary drying, the chamber pressure is lowered to a set value, and the shelf temperature is increased to deliver the necessary heat for the sublimation process. The product temperature increases until the equilibrium pressure of ice succeeds the chamber pressure. The energy input into the product depends on the process conditions, mainly from the shelf temperature and chamber pressure. In primary drying, the direction of the heat transfer switches. The shelf temperature transfers heat into the product that is transported by conduction to the sublimation interface and is then consumed by sublimation.

The difference in the heat flux based on the process conditions can be seen in Figure 15. Here, the experiments have been conducted twice. At aggressive process conditions, the heat flow into the product rises strongly until it reaches its maximum of 295 W/m^2 and then slowly descends. As soon as the maximum heat flow is reached, sublimation occurs. It is an endothermic process that requires constant heat input. At a shelf temperature of $0\text{ }^{\circ}\text{C}$ and 0.3 mbar , the heat transfer into the product is so high that not all energy is required for sublimation, leading to a product temperature increase. A more conservative process design shows a smaller amount of heat transferred into the product. Here the maximum lies at 50 W/m^2 . This leads to very long primary drying times compared with more aggressive cycles.

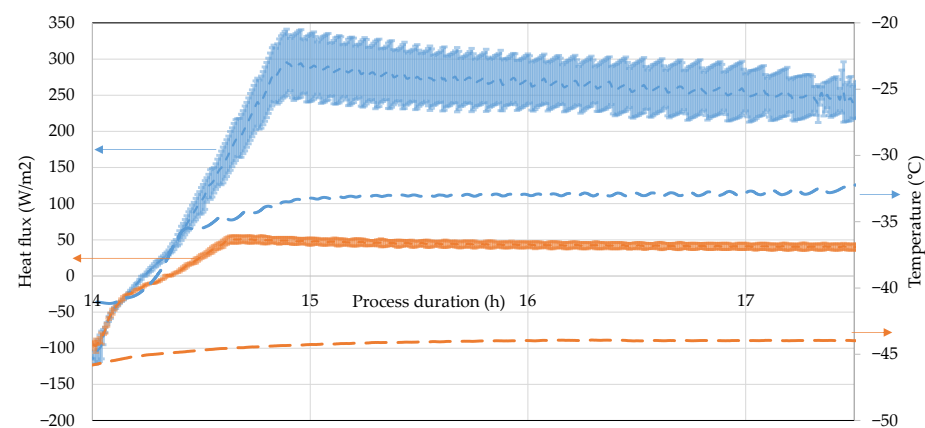


Figure 15. Heat flux and product temperature are based on different process conditions.

The heat flow sensor is able to measure the heat flow between the product and the shelf in a physically meaningful way based on the different process conditions. This could allow online measurement of the vial heat transfer coefficient during primary drying. The heat transfer coefficient has been determined by ice sublimation tests and by means of heat flux measurement for different process conditions. The used equation for the heat flux measurement is [45]

$$K_v = \frac{J_{Heat\ flux}}{(T_S - T_p)} \quad (3)$$

Figure 16 shows the different obtained values for the heat transfer coefficients. At $-25\text{ }^\circ\text{C}$, edge vials have a significantly higher heat transfer coefficient than center vials or the measured edge vial with heat flux. Generally, the heat flux K_v is significantly lower than the other two values. At a shelf temperature of $-25\text{ }^\circ\text{C}$, the edge K_v has a value of $18.6\text{ W}/(\text{m}^2\text{ K})$ (0.05 mbar) and $34.3\text{ W}/(\text{m}^2\text{ K})$ (0.3 mbar), while the heat flux K_v has respective values of $2.1\text{ W}/(\text{m}^2\text{ K})$ (0.05 mbar) and $6.6\text{ W}/(\text{m}^2\text{ K})$ (0.3 mbar). This is because the heat flux sensor only measures the heat flow from the shelf into the product, but during lyophilization, radiative heat transfer from the chamber walls and heat conduction from the tray or other vials also play a role, as found by other authors [42].

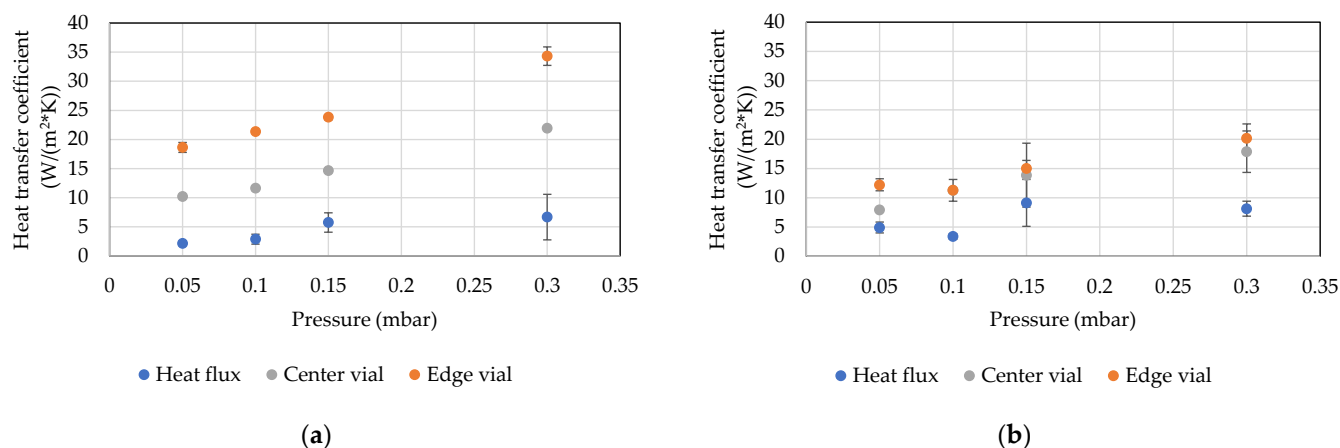


Figure 16. Heat transfer coefficients for different process conditions and vials (a) $-25\text{ }^\circ\text{C}$ (b) $0\text{ }^\circ\text{C}$.

With increasing shelf temperature, the edge effect decreases, and the drying behavior between the vials becomes more homogeneous. Edge and center vials show similar values, but the heat flux K_v is still much smaller and shows no big change in value. The heat flux K_v increases with increasing chamber pressure, similar to the values from the ice sublimation tests because of the increased gas conduction. The edge K_v has a value of $12.2\text{ W}/(\text{m}^2\text{ K})$ (0.05 mbar) and $20.2\text{ W}/(\text{m}^2\text{ K})$ (0.3 mbar) while the center K_v has respective values of $8\text{ W}/(\text{m}^2\text{ K})$ (0.05 mbar) and $17.8\text{ W}/(\text{m}^2\text{ K})$ (0.3 mbar). At this pressure value, the heat flux K_v deviates 60% from the edge vial and around 40% from the center vial K_v at both pressure values.

Since the heat flux sensor constantly measures the heat flux, an online determination of the heat transfer coefficient is possible. The heat transfer data over the primary drying duration for given process conditions are shown in Figure 17. At first, the value fluctuates strongly. Here occurs no sublimation. As soon as sublimation occurs, the value establishes itself at $5.7 \pm \text{ca.}2\text{ W}/(\text{m}^2\text{ K})$. The experiment has been conducted twice. The assumption of a constant value for the heat transfer coefficient during steady-state modeling is reasonable.

Since the product temperature slowly increases and subsequently reaches the shelf temperature, the endpoint of primary drying can be detected by the heat flux sensor. As soon as the heat flux data fall below zero, the direction of heat flow changes again, and no sublimation occurs. For this measurement to be accurate, the vial bottom must be placed precisely on the heat flux sensor. In Figure 18, the heat flux data can be seen for the primary and secondary drying where 5 g/L Saccharose has a detected endpoint at 13.5 h,

25 g/L at 18.9 h, and 100 g/L at 3.8 h. The last endpoint is unrealistic since the increased solute concentration leads to a slower sublimation rate causing a longer primary drying. Therefore, the vial has to be carefully placed on the heat flux sensor to obtain reliable data.

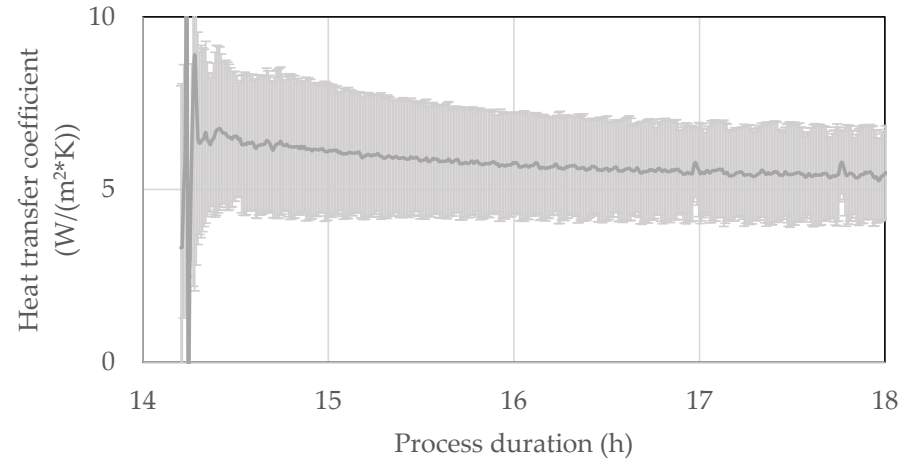


Figure 17. Vial heat transfer coefficient during primary drying duration measured with heat flux sensor ($T_s = -25\text{ }^\circ\text{C}$, $p_c = 0.15\text{ mbar}$).

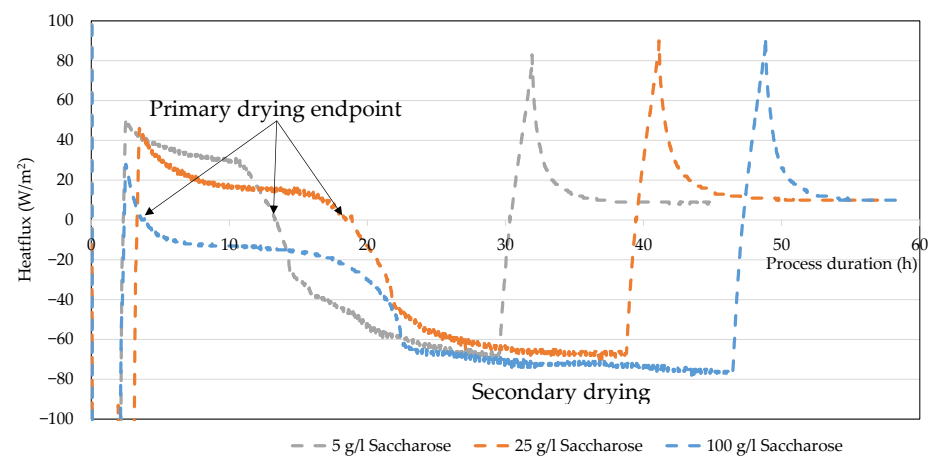


Figure 18. Heat flux data over primary and secondary drying of saccharose solutions with different concentrations.

During secondary drying, the shelf temperature is further increased to accelerate the desorption of water. In Figure 18, the heat flux profiles are shown. At first, the fluxes increase drastically. The values of the maxima are similar for the three solute concentrations laying between 81 to 90 W/m^2 and then rapidly decreasing to 10 W/m^2 for all solute concentrations, leading to the conclusion that only a small amount of energy is supplied for desorption in the holding step of secondary drying.

4.5. Ice Ruler

During primary drying, the ice occupation on the ice condenser rises as water vapor from the sublimation process resublimates. Here the ice ruler measures the ice height. In Figure 19, the ice ruler is shown at different points during the process. At the start of the freezing process, no ice is on the ice condenser. During the freezing step, water vapor that is inside the chamber is deposited on the ice condenser. The main increase in ice on the ice condenser happens during the primary drying phase. Here, ice in the product is sublimed, and the generated water vapor is resublimed on the ice condenser, leading to an increase in the ice occupation.

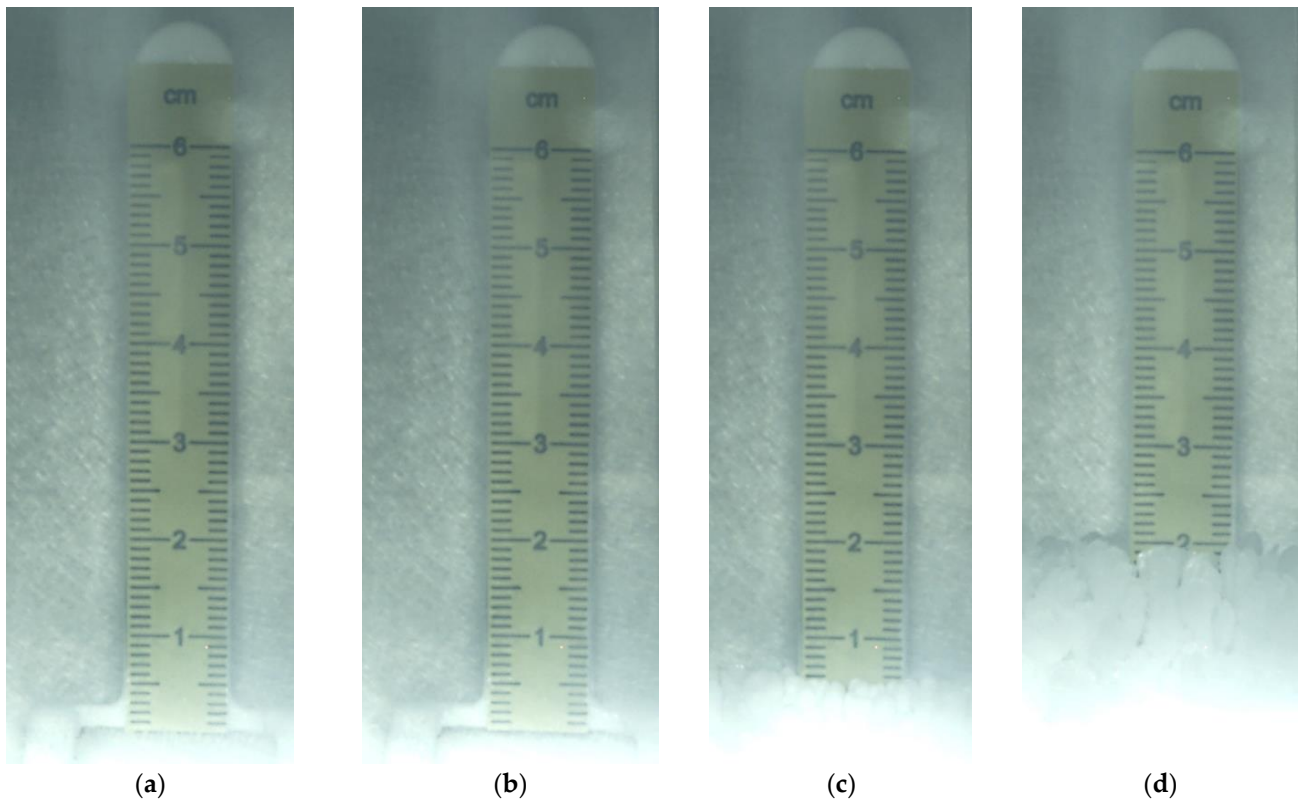


Figure 19. Ice ruler occupation with ongoing freeze drying duration: (a) experiment start, (b) start of primary drying, (c) further primary drying, and (d) end of primary drying.

The ice ruler measures the ice occupation over time, which is dependent on the sublimation rate, while the sublimation rate is a function of shelf temperature and chamber pressure. Figure 20 shows the ice occupation over time for different process conditions. At a chamber pressure of 0.05 mbar, the ice heights of the three tested shelf temperatures are comparable. An ice height of 0.1 cm is reached at 15.38 ± 0.45 h (0°C), 14.7 ± 0.11 h (-12.5°C) and 14.26 ± 0.01 h (-25°C). During the primary drying process, the ice height increases. A height of 0.4 cm is reached after 18 ± 0.05 h (0°C), 18.35 ± 0.7 h (-12.5°C) and 18.45 ± 0.48 h (-25°C).

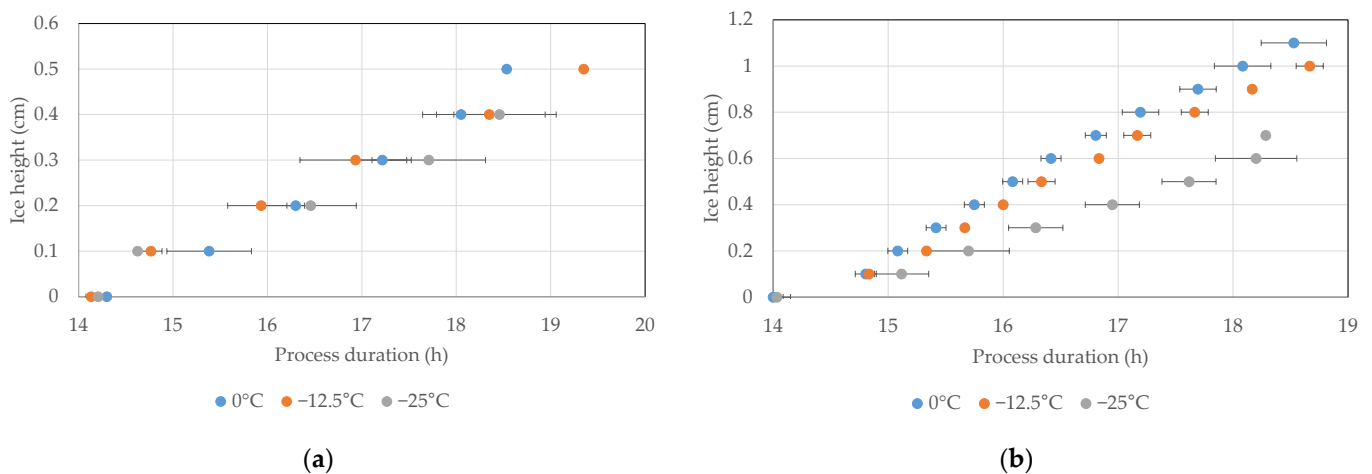


Figure 20. Ice occupation over primary drying time for ice sublimation tests (a) 0.05 mbar and (b) 0.3 mbar.

With an increase in chamber pressure, a difference in different shelf temperatures can be seen. Higher chamber pressure reduces the driving force for sublimation but increases the heat transfer into the product, leading to an increased equilibrium pressure, which, in turn, increases the driving force again. For all shelf temperatures, the ice height increased during the same period of time, and 0.1 cm ice height was reached at 14.8 ± 0.09 h (0 °C), 14.83 ± 0.03 h (-12.5 °C), and 15.12 ± 0.24 h (-25 °C). The increasing difference between the ice heights becomes more eminent with increasing primary drying time. A height of 0.6 cm is reached after 16.4 ± 0.09 h (0 °C), 16.8 ± 0.01 h (-12.5 °C) and 18.2 ± 0.35 h (-25 °C). The smaller heat input from the lower shelf temperature has a smaller influence at lower chamber pressure since, here, a sufficient driving force is already set with the chamber pressure. At higher chamber pressure, the heat input increases, leading to accelerated sublimation rates compared with lower chamber pressure, and with increasing shelf temperature, the temperature-dependent equilibrium pressure of ice further increases, leading to an even more accelerated sublimation.

The ice ruler is able to measure the ice height based on different process parameters in a physically meaningful manner. Aggressive cycles show a faster ice occupation.

In Figure 21, the ice height over time for different solute concentrations is shown. As discussed before, the dry layer resistance increases with the solute concentration. Therefore, at the same process conditions, the higher solute concentrations have a lower sublimation rate. This causes a slower growth of the ice on the ice condenser. At 5 g/L solute, the ice height increases linearly and then quickly approaches the final value, while at 100 g/L, the initial increase is also linear, and then the ice height slowly increases to the end value. During secondary drying, no increase in ice height is detectable.

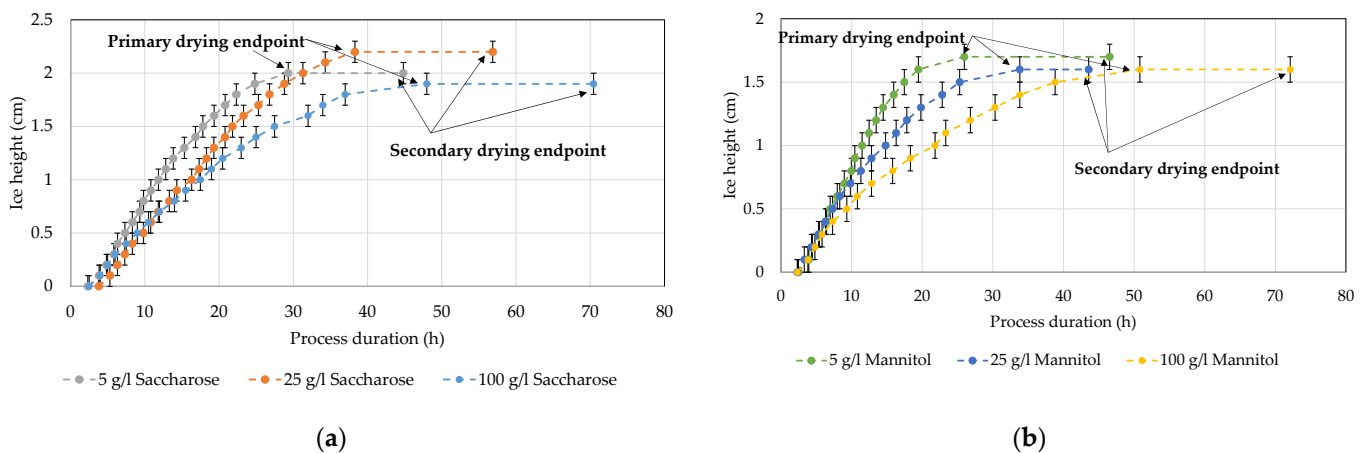


Figure 21. Ice height over time measured by an ice ruler for different solute concentrations of (a) saccharose and (b) mannitol.

Next, the results for different solute concentrations are compared with the sublimation rate measured by MTM. In Figure 22, the sublimated ice mass and the ice height over the course of the process are shown. The progression of ice height and sublimated mass are comparable for all solute concentrations. At 100 g/L, MTM shows high deviations for both solutes. The increased batch heterogeneity leads to uncertainty in the number of vials that are sublimating, causing variance in the measurement. The course of the ice ruler is in good agreement with the sublimation rate. As soon as no increase in ice height is detectable, the primary drying phase is completed.

Since the ice ruler is a batch method, the endpoint is compared with the endpoint by comparative pressure measurement for different solutions. Increasing concentrations lead to longer primary drying. Figure 23 shows the primary drying endpoints as a parity plot. The endpoint of the ice ruler and comparative pressure are in very good agreement.

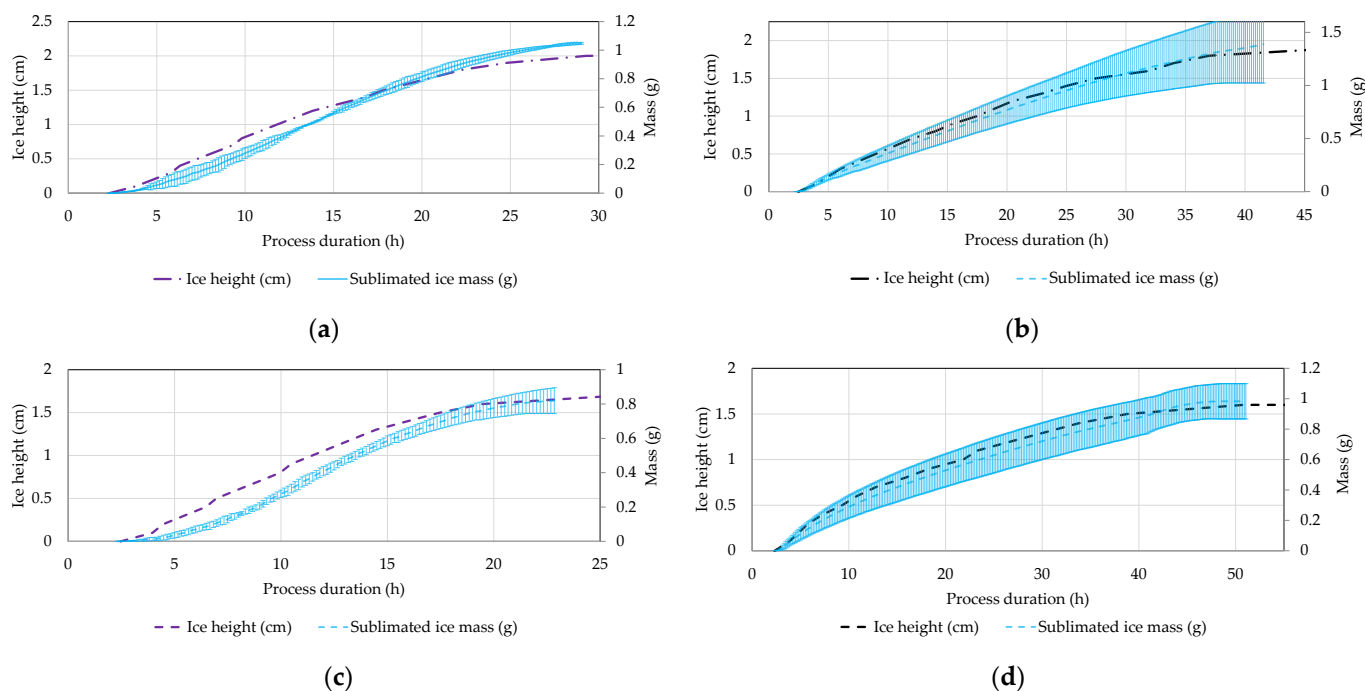


Figure 22. Sublimated mass and ice height (a) 5 g/L saccharose, (b) 100 g/L saccharose, (c) 5 g/L mannitol, (d) 100 g/L mannitol.

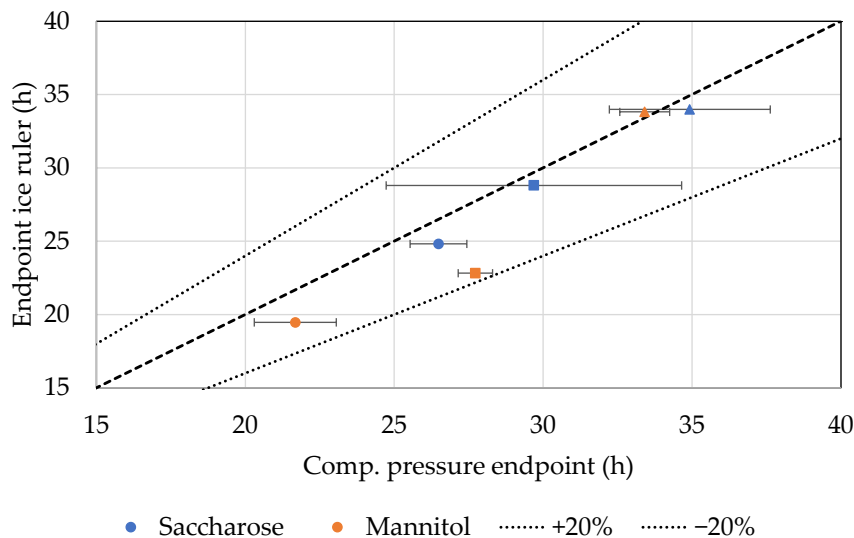


Figure 23. Primary drying endpoint of ice ruler and comparative pressure measurements (round—5 g/L, square—25 g/L, and triangle—100 g/L).

5. Discussion

In this work, different PAT tools are tested with different concentrations of an amorphous and crystalline excipient.

WTMplus sensors measure the product temperature. Their high flexibility in placement and their compatibility with automatic loading systems are advantages to the most commonly used thermocouples and allow precise temperature measurements of the probed vial inside the batch with 0.1 K deviation. However, the invasive nature of the sensor remains and could result in atypical drying of the vial.

The combination of Pirani and capacitive pressure sensors is called comparative pressure measurement. It can reliably detect the endpoint of primary drying of the batch, given the difference in measurement principle, and shows high potential as PAT for primary drying

endpoint determination. Depending on the recipe, a time saving of 30% is possible [7]. Furthermore, it has been shown that a qualitative assessment of batch heterogeneity is possible based on the slope of the pressure signal.

MTM is an adaptation of the pressure rise test. It can determine the vapor pressure of ice at the sublimation front, the dry layer resistance, and the primary drying endpoint. The dry layer resistance can be reproducibly determined for different process conditions and solute concentrations with relative deviations of up to 30% in measurement time. The primary drying endpoint is in good agreement with comparative pressure measurement onset, with a difference of 10 to 15% in time. During the measurement, the chamber pressure rises. This could cause a product temperature increase. The optimized MTM stops the measurement as soon as no pressure increase is detected, leading to a significantly reduced measurement time of 5.7 s, ensuring product safety during the measurement. The noninvasive online measurement and the combination with process modeling make it a powerful tool for advanced process control where the product temperature and primary drying endpoint can be determined noninvasively for every vial, bridging the gap between the combination of invasive temperature measurement and batch methods.

Heat flux measurement is used to detect different thermal events during the freeze-drying process, as it can noninvasively detect the nucleation time of batches. Furthermore, it is possible to determine the heat transfer coefficient during freeze-drying runs for predictive process modeling, but it has been shown that the value is underestimated by approximately 35–70% at 0 °C and 60–80% at –25 °C shelf temperature. Here, more experimental work with different equipment configurations, such as radiation shields and partial loading, must be carried out in order to find the major cause of the deviation and to optimize the measurement. The heat flow into the product can be reliably measured with different process conditions, and endpoint determination of the observed vial is also possible with approximately 1–33% accuracy. The results are in good agreement with the experiments, but the accurate placement of the vial on the sensor is crucial.

The newly developed *ice ruler* allows the measurement of the ice height on the ice condenser. It has been shown above that the ice increase is directly correlated with the process conditions: aggressive conditions lead to increased ice growth rates, while an increase in solute concentration decreases the ice growth rate. The resulting height curves are compared with the sublimated ice mass determined by MTM. The progressions are in good agreement. The ice ruler additionally allows primary drying endpoint determination, and the results are in good agreement with the comparative pressure measurement by approximately 6–17%. Since the water content in secondary drying is low, no significant ice increase could be detected here. To implement the ice ruler as a PAT, an image analysis algorithm needs to be implemented that will allow the evaluation of the ice height during the process.

Different PATs for lyophilization have been presented in this paper. Their usability has been shown, and their shortcomings discussed. The combination of comparative pressure measurement and MTM as a PAT is recommended for distinct endpoint determination of primary drying. MTM can be used for accelerated model parameter determination for process optimization by modeling the model parameter R_p . The vial heat transfer coefficient can be detected with the heat flux sensor, but the value is underestimated; therefore, currently, it cannot be completely recommended for this usage. However, it can be used as PAT in the freezing step to determine the nucleation temperature and the endpoint of freezing. A combination with a PAT for controlled nucleation would be useful to measure whether the nucleation temperatures of the vials are the same. The ice ruler showed good agreement with the results of MTM and can additionally be used for endpoint determination, besides MTM and comparative pressure measurement, as soon as an evaluation algorithm exists. The necessary equipment and the usability for different objectives are summarized in Table 5 for the investigated PAT tools.

Table 5. PAT tools and their recommendation for usage in process control (green—fully recommended, yellow—limited recommendation, and orange—more experience necessary).

PAT Tool	Necessary Equipment	Objective	Rec.	Remarks
WTM	WTMplus sensor Transponder	Product temperature determination		Major advantages over wired sensors but invasive
Comp. pressure	Pirani gauge Capacitive sensor	Pressure control		Pressure control can be obtained by either sensor Pirani: gas-type-dependent Capacitive: gas-type-independent
		Primary drying endpoint		Measures endpoint of the whole batch
MTM	Two-chamber freeze dryer with closable intermediate valve Analysis tool	Model parameter determination R_p		Noninvasive online measurement, value valid until 2/3 of primary drying
		Primary drying endpoint		Pressure rise can induce melt back if the recipe is too aggressive Optimized MTM for reduced measurement time
Heat flux	Heat flux sensor Datalogger Readout software	Nucleation temperature determination		Only measurement possible; combination with controlled nucleation required
		Model parameter determination K_v		Value significantly underestimated; more experience must be gained
		Primary drying endpoint		Value in good agreement with WTM but exact positioning necessary
Ice ruler	Ice ruler Camera Analysis tool	Primary drying endpoint		Sublimated ice mass in good agreement with ice occupation Analysis algorithm required

Any process control strategy aiming at the advanced process control of the freezing and primary step should include controlled nucleation, heat flux, comparative pressure, and MTM. The control of the secondary drying steps is more sophisticated, and fewer tools are available: MS [49], TDLAS [18,62], and PRT/MTM [53,62].

Author Contributions: A.J. was responsible for methodology, experimental design, and evaluation and wrote this paper. P.K. and F.H. supported laboratory and piloting equipment as well as with expert knowledge regarding operations and objectives. J.S. was responsible for conception and supervision. All authors have read and agreed to the published version of the manuscript.

Funding: This research received no external funding.

Acknowledgments: The authors would like to thank Ahmad Alsouriti, formerly a student at TU Clausthal, for his considerate and accurate laboratory work in conducting experiments. The authors acknowledge support from the Open Access Publishing Fund of the Clausthal University of Technology.

Conflicts of Interest: The authors declare no conflict of interest. The company had no role in the design of the study; in the collection, analyses, or interpretation of data; in the writing of the manuscript, and in the decision to publish the results.

References

- Kawasaki, H.; Shimanouchi, T.; Kimura, Y. Recent Development of Optimization of Lyophilization Process. *J. Chem.* **2019**, *2019*, 9502856. [CrossRef]
- Tang, X.C.; Pikal, M.J. Design of Freeze-Drying Processes for Pharmaceuticals: Practical Advice. *Pharm. Res.* **2004**, *21*, 191–200. [CrossRef]
- Greiff, D. Development of cycles for lyophilization. *Dev. Biol. Stand.* **1992**, *74*, 85–92.
- FDA. PAT—A Framework for Innovative Pharmaceutical Development, Manufacturing, and Quality Assurance. FDA [Online], June 11. Available online: <https://www.fda.gov/regulatory-information/search-fda-guidance-documents/pat-framework-innovative-pharmaceutical-development-manufacturing-and-quality-assurance> (accessed on 15 February 2021).
- European Medicines Agency. ICH Guideline Q8 (R2) on Pharmaceutical Development. Available online: https://www.ema.europa.eu/en/documents/scientific-guideline/international-conference-harmonisation-technical-requirements-registration-pharmaceuticals-human-use_en-11.pdf (accessed on 24 June 2022).
- Helgers, H.; Schmidt, A.; Lohmann, L.J.; Vetter, F.L.; Juckers, A.; Jensch, C.; Mouellef, M.; Zobel-Roos, S.; Strube, J. Towards Autonomous Operation by Advanced Process Control—Process Analytical Technology for Continuous Biologics Antibody Manufacturing. *Processes* **2021**, *9*, 172. [CrossRef]

7. Juckers, A.; Knerr, P.; Harms, F.; Strube, J. Advanced Process Analytical Technology in Combination with Process Modeling for Endpoint and Model Parameter Determination in Lyophilization Process Design and Optimization. *Processes* **2021**, *9*, 1600. [[CrossRef](#)]
8. Klepzig, L.S.; Juckers, A.; Knerr, P.; Harms, F.; Strube, J. Digital Twin for Lyophilization by Process Modeling in Manufacturing of Biologics. *Processes* **2020**, *8*, 1325. [[CrossRef](#)]
9. Juckers, A.; Knerr, P.; Harms, F.; Strube, J. Model-Based Product Temperature and Endpoint Determination in Primary Drying of Lyophilization Processes. *Pharmaceutics* **2022**, *14*, 809. [[CrossRef](#)]
10. Willemer, H. Measurements of temperatures, ice evaporation rates and residual moisture contents in freeze-drying. *Dev. Biol. Stand.* **1992**, *74*, 123–134; discussion 135–136.
11. Schneid, S.; Gieseler, H. Evaluation of a New Wireless Temperature Remote Interrogation System (TEMPRIS) to Measure Product Temperature During Freeze Drying. *AAPS PharmSciTech* **2008**, *9*, 729–739. [[CrossRef](#)]
12. Moino, C.; Bourlés, E.; Pisano, R.; Scutellà, B. In-Line Monitoring of the Freeze-Drying Process by Means of Heat Flux Sensors. *Ind. Eng. Chem. Res.* **2021**, *60*, 9637–9645. [[CrossRef](#)]
13. Chen, R.; Slater, N.K.; Gatlin, L.A.; Kramer, T.; Shalaev, E.Y. Comparative Rates of Freeze-Drying for Lactose and Sucrose Solutions as Measured by Photographic Recording, Product Temperature, and Heat Flux Transducer. *Pharm. Dev. Technol.* **2008**, *13*, 367–374. [[CrossRef](#)]
14. De Beer, T.R.M.; Vercruyssen, P.; Burggraef, A.; Quinten, T.; Ouyang, J.; Zhang, X.; Vervaet, C.; Remon, J.P.; Baeyens, W.R.G. In-line and real-time process monitoring of a freeze drying process using Raman and NIR spectroscopy as complementary process analytical technology (PAT) tools. *J. Pharm. Sci.* **2009**, *98*, 3430–3446. [[CrossRef](#)] [[PubMed](#)]
15. Brülls, M.; Folestad, S.; Sparén, A.; Rasmuson, A. In-situ near-infrared spectroscopy monitoring of the lyophilization process. *Pharm. Res.* **2003**, *20*, 494–499. [[CrossRef](#)]
16. Presser, I. *Innovative Online Messverfahren Zur Optimierung Von Gefriertrocknungsprozessen*; Ludwig-Maximilians-Universität München: München, France, 2003.
17. Antonello, A.B.; Fissore, D. In-Line Product Quality Control of Pharmaceuticals in Freeze-Drying Processes. In *Modern Drying Technology*; John Wiley & Sons, Ltd.: Hoboken, NJ, USA, 2011; pp. 91–154.
18. Patel, S.M.; Pikal, M. Process Analytical Technologies (PAT) in freeze-drying of parenteral products. *Pharm. Dev. Technol.* **2009**, *14*, 567–587. [[CrossRef](#)]
19. Read, E.; Shah, R.; Riley, B.; Park, J.; Brorson, K.; Rathore, A. Process analytical technology (PAT) for biopharmaceutical products: Part II. Concepts and applications. *Biotechnol. Bioeng.* **2009**, *105*, 285–295. [[CrossRef](#)]
20. Fissore, D.; Pisano, R.; Barresi, A.A. Process analytical technology for monitoring pharmaceuticals freeze-drying—A comprehensive review. *Dry. Technol.* **2018**, *36*, 1839–1865. [[CrossRef](#)]
21. Patel, S.M.; Doen, T.; Pikal, M.J. Determination of End Point of Primary Drying in Freeze-Drying Process Control. *AAPS PharmSciTech* **2010**, *11*, 73–84. [[CrossRef](#)]
22. Patel, S.M.; Jameel, F.; Pikal, M.J. The Effect of Dryer Load on Freeze Drying Process Design. *J. Pharm. Sci.* **2010**, *99*, 4363–4379. [[CrossRef](#)]
23. Zhou, D.; Shang, S.; Tharp, T.; Jameel, F.; Sinha, K.; Nere, N.K. Leveraging Lyophilization Modeling for Reliable Development, Scale-up and Technology Transfer. *AAPS PharmSciTech* **2019**, *20*, 263. [[CrossRef](#)]
24. Wigenhorn, M.; Presser, I.; Winter, G. The current state of PAT in freeze-drying. *Am. Pharm. Rev.* **2005**, *8*, 38–44.
25. Tang, X.; Nail, S.L.; Pikal, M.J. Evaluation of manometric temperature measurement, a process analytical technology tool for freeze-drying: Part I, product temperature measurement. *AAPS PharmSciTech* **2006**, *7*, E95–E103. [[CrossRef](#)]
26. Tang, X.C.; Nail, S.L.; Pikal, M.J. Evaluation of manometric temperature measurement (MTM), a process analytical technology tool in freeze drying, part III: Heat and mass transfer measurement. *AAPS PharmSciTech* **2006**, *7*, E105–E111. [[CrossRef](#)]
27. Gieseler, H.; Kramer, T.; Pikal, M.J. Use of manometric temperature measurement (MTM) and SMART™ freeze dryer technology for development of an optimized freeze-drying cycle. *J. Pharm. Sci.* **2007**, *96*, 3402–3418. [[CrossRef](#)] [[PubMed](#)]
28. Schneid, S. *Investigation of Novel Process Analytical Technology (PAT) Tools for Use in Freeze-Drying Processes: Doctoralthesis*; Friedrich-Alexander-Universität Erlangen-Nürnberg (FAU): Erlangen, Germany, 2009.
29. Wegiel, L.A.; Ferris, S.J.; Nail, S.L. Experimental Aspects of Measuring the Vial Heat Transfer Coefficient in Pharmaceutical Freeze-Drying. *AAPS PharmSciTech* **2018**, *19*, 1810–1817. [[CrossRef](#)] [[PubMed](#)]
30. Ari, K. *Raman and Near-Infrared Spectroscopic Methods for In-Line Monitoring of Freeze-Drying Process*; University of Eastern Finland: Joensuu, Finland, 2015; ISBN 78-952-61-1717-1.
31. Grohgan, H.; Gildemyn, D.; Skibsted, E.; Flink, J.M.; Rantanen, J. Rapid Solid-State Analysis of Freeze-Dried Protein Formulations Using NIR and Raman Spectroscopies. *J. Pharm. Sci.* **2011**, *100*, 2871–2875. [[CrossRef](#)]
32. Kauppinen, A.; Toiviainen, M.; Aaltonen, J.; Korhonen, O.; Järvinen, K.; Juuti, M.; Pellinen, R.; Ketolainen, J. Microscale Freeze-Drying with Raman Spectroscopy as a Tool for Process Development. *Anal. Chem.* **2013**, *85*, 2109–2116. [[CrossRef](#)]
33. Pieters, S.; Heyden, Y.V.; Roger, J.-M.; D’Hondt, M.; Hansen, L.; Palagos, B.; De Spiegeleer, B.; Remon, J.-P.; Vervaet, C.; De Beer, T. Raman spectroscopy and multivariate analysis for the rapid discrimination between native-like and non-native states in freeze-dried protein formulations. *Eur. J. Pharm. Biopharm.* **2013**, *85*, 263–271. [[CrossRef](#)]
34. Preskar, M.; Korasa, K.; Vrbanec, T.; Klement, D.; Vrečer, F.; Gašperlin, M. Applicability of Raman and near-infrared spectroscopy in the monitoring of freeze-drying injectable ibuprofen. *Drug Dev. Ind. Pharm.* **2021**, *47*, 758–769. [[CrossRef](#)]

35. Romero-Torres, S.; Wikström, H.; Grant, E.R.; Taylor, L.S. Monitoring of mannitol phase behavior during freeze-drying using non-invasive Raman spectroscopy. *PDA J. Pharm. Sci. Technol.* **2007**, *61*, 131–145.
36. Sampathkumar, K.; Cao, W.; Phillips, J.; Amgen, P. Applying Raman Spectroscopy to Design of Lyophilization Cycles for Protein Formulation Development. *Am. Pharm. Rev.* **2009**, *12*, 44–48.
37. Sarraguça, M.C.; De Beer, T.; Vervaet, C.; Remon, J.-P.; Lopes, J.A. A batch modelling approach to monitor a freeze-drying process using in-line Raman spectroscopy. *Talanta* **2010**, *83*, 130–138. [[CrossRef](#)]
38. Su, W.; Hao, H.; Glennon, B.; Barrett, M. Spontaneous Polymorphic Nucleation of d-Mannitol in Aqueous Solution Monitored with Raman Spectroscopy and FBRM. *Cryst. Growth Des.* **2013**, *13*, 5179–5187. [[CrossRef](#)]
39. De Beer, T.; Burggraeve, A.; Fonteyne, M.; Saerens, L.; Remon, J.; Vervaet, C. Near infrared and Raman spectroscopy for the in-process monitoring of pharmaceutical production processes. *Int. J. Pharm.* **2011**, *417*, 32–47. [[CrossRef](#)]
40. De Beer, T.R.M.; Allesø, M.; Goethals, F.; Coppens, A.; Heyden, Y.V.; De Diego, H.L.; Rantanen, J.; Verpoort, F.; Vervaet, C.; Remon, A.J.P.; et al. Implementation of a Process Analytical Technology System in a Freeze-Drying Process Using Raman Spectroscopy for In-Line Process Monitoring. *Anal. Chem.* **2007**, *79*, 7992–8003. [[CrossRef](#)]
41. De Beer, T.; Wiggenhorn, M.; Hawe, A.; Kasper, J.; Almeida, A.; Quinten, T.; Friess, W.; Winter, G.; Vervaet, C.; Remon, J. Optimization of a pharmaceutical freeze-dried product and its process using an experimental design approach and innovative process analyzers. *Talanta* **2011**, *83*, 1623–1633. [[CrossRef](#)]
42. Carfagna, M.; Rosa, M.; Hawe, A.; Frieß, W. Design of freeze-drying cycles: The determination of heat transfer coefficient by using heat flux sensor and MicroFD. *Int. J. Pharm.* **2022**, *621*, 121763. [[CrossRef](#)]
43. Vollrath, I. *Controlled Nucleation and Heat Flux Measurements as Innovative Technologies for Freeze-Drying*; Ludwig-Maximilians-Universität München: München, Germany, 2018.
44. Vollrath, I.; Pauli, V.; Friess, W.; Freitag, A.; Hawe, A.; Winter, G. Evaluation of Heat Flux Measurement as a New Process Analytical Technology Monitoring Tool in Freeze Drying. *J. Pharm. Sci.* **2017**, *106*, 1249–1257. [[CrossRef](#)]
45. Carfagna, M.; Rosa, M.; Lucke, M.; Hawe, A.; Frieß, W. Heat flux sensor to create a design space for freeze-drying development. *Eur. J. Pharm. Biopharm.* **2020**, *153*, 84–94. [[CrossRef](#)]
46. Mayeresse, Y.; Veillon, R.; Sibille, P.H.; Nomine, C. Freeze-drying process monitoring using a cold plasma ionization device. *PDA J. Pharm. Sci. Technol.* **2007**, *61*, 160–174.
47. Barresi, A.; Pisano, R.; Fissore, D.; Rasetto, V.; Velardi, S.A.; Vallan, A.; Parvis, M.; Galan, M. Monitoring of the primary drying of a lyophilization process in vials. *Chem. Eng. Process. Process Intensif.* **2009**, *48*, 408–423. [[CrossRef](#)]
48. Assegehegn, G.; la Fuente, E.B.-D.; Franco, J.M.; Gallegos, C. Freeze-drying: A relevant unit operation in the manufacture of foods, nutritional products, and pharmaceuticals. *Adv. Food Nutr. Res.* **2020**, *93*, 1–58. [[CrossRef](#)]
49. Ganguly, A.; Stewart, J.; Rhoden, A.; Volny, M.; Saad, N. Mass spectrometry in freeze-drying: Motivations for using a bespoke PAT for laboratory and production environment. *Eur. J. Pharm. Biopharm.* **2018**, *127*, 298–308. [[CrossRef](#)]
50. Fissore, D.; Pisano, R.; Barresi, A. On the Methods Based on the Pressure Rise Test for Monitoring a Freeze-Drying Process. *Dry. Technol.* **2010**, *29*, 73–90. [[CrossRef](#)]
51. Lewis, L.M.; Johnson, R.E.; Oldroyd, M.E.; Ahmed, S.S.; Joseph, L.; Saracovan, I.; Sinha, S. Characterizing the Freeze-Drying Behavior of Model Protein Formulations. *AAPS PharmSciTech* **2010**, *11*, 1580–1590. [[CrossRef](#)]
52. Milton, N.; Pikal, M.J.; Roy, M.L.; Nail, S.L. Evaluation of manometric temperature measurement as a method of monitoring product temperature during lyophilization. *PDA J. Pharm. Sci. Technol.* **1997**, *51*, 7–16.
53. Tang, X.C.; Nail, S.L.; Pikal, M.J. Freeze-Drying Process Design by Manometric Temperature Measurement: Design of a Smart Freeze-Dryer. *Pharm. Res.* **2005**, *22*, 685–700. [[CrossRef](#)]
54. Tang, X.C.; Nail, S.L.; Pikal, M.J. Evaluation of manometric temperature measurement, a process analytical technology tool for freeze-drying: Part II measurement of dry-layer resistance. *AAPS PharmSciTech* **2006**, *7*, E77–E84. [[CrossRef](#)]
55. Awotwe-Otoo, D.; Agarabi, C.; Khan, M.A. An Integrated Process Analytical Technology (PAT) Approach to Monitoring the Effect of Supercooling on Lyophilization Product and Process Parameters of Model Monoclonal Antibody Formulations. *J. Pharm. Sci.* **2014**, *103*, 2042–2052. [[CrossRef](#)]
56. Gieseler, H.; Kessler, W.J.; Finson, M.; Davis, S.J.; Mulhall, P.A.; Bons, V.; Debo, D.J.; Pikal, M.J. Evaluation of tunable diode laser absorption spectroscopy for in-process water vapor mass flux measurements during freeze drying. *J. Pharm. Sci.* **2007**, *96*, 1776–1793. [[CrossRef](#)]
57. Kuu, W.Y.; Nail, S.L. Rapid freeze-drying cycle optimization using computer programs developed based on heat and mass transfer models and facilitated by tunable diode laser absorption spectroscopy (TDLAS). *J. Pharm. Sci.* **2009**, *98*, 3469–3482. [[CrossRef](#)]
58. Kuu, W.Y.; O'Bryan, K.R.; Hardwick, L.M.; Paul, T.W. Product mass transfer resistance directly determined during freeze-drying cycle runs using tunable diode laser absorption spectroscopy (TDLAS) and pore diffusion model. *Pharm. Dev. Technol.* **2010**, *16*, 343–357. [[CrossRef](#)]
59. Jameel, F.; Kessler, W.J.; Schneid, S. Application of PAT in Real-time Monitoring and Controlling of Lyophilization Process. In *Quality by Design for Biopharmaceutical Drug Product Development*; Jameel, F., Hershenson, S., Khan, M.A., Martin-Moe, S., Eds.; Springer: New York, NY, USA, 2015; pp. 605–647. ISBN 978-1-4939-2315-1.

60. Kessler, W.J.; Gong, E. Tunable Diode Laser Absorption Spectroscopy in Lyophilization. In *Lyophilization of Pharmaceuticals and Biologicals*; Ward, K.R., Matejtschuk, P., Eds.; Springer: New York, NY, USA, 2019; pp. 113–141. ISBN 978-1-4939-8927-0.
61. Sharma, P.; Kessler, W.J.; Bogner, R.; Thakur, M.; Pikal, M.J. Applications of the Tunable Diode Laser Absorption Spectroscopy: In-Process Estimation of Primary Drying Heterogeneity and Product Temperature During Lyophilization. *J. Pharm. Sci.* **2018**, *108*, 416–430. [[CrossRef](#)]
62. Fissore, D.; Pisano, R.; Barresi, A.A. Monitoring of the Secondary Drying in Freeze-Drying of Pharmaceuticals. *J. Pharm. Sci.* **2011**, *100*, 732–742. [[CrossRef](#)]